International M2 Atmospheric Environment (2016-2017)

Internship Report

First study of night-time aerosol properties and variability in the Dakar site

Supervisor: Philippe GOLOUB Student: Miaomiao ZHU

Laboratoire d'Optique Atmosphérique (LOA)

Université de Lille 1, France

June 12th, 2017

Table of Contents

Acknowledgements

First of all, I would like to give my deepest gratitude to my supervisor, Philippe Goloub, for his constant encouragement and guidance during my internship. Prof. Goloub has walked me through every stage of my work with great patience. Without his illuminating instruction, this report couldn't reach its present form.

Second, I would like to extend my sincere gratitude to PHD students Ioana Popovici and Qiaoyun Hu. Thanks for providing me lots of sources and giving me great help in improving my professional skills. I feel so lucky to have the chance to work in this creative team.

Many thanks to engineer Christine Deroo for even spending her weekends to re-process Lidar inversions so that I can obtain these data in time.

I also would like to express my heartfelt thanks to engineer Fabric Ducos, secretary Anne Prime, engineer Romain de Filippe and many other stuffs in LOA who give me lots of help during my work here.

I also owe my most sincere gratitude to all of my professors and my fellow classmates in this M2 program, who spent lots of time in helping me work out my problems of difficult courses and go through a lot of happy moments with me. Special thanks to my one of my most talent fellow classmate Dumitru Duca who help me a lot with my courses and exams after class.

And I very appreciate CaPPA for providing me this opportunity and supporting me to study and do internship here.

Thanks to my friends also the PHD students Fangwen Bao, Cheng Chen, Lei Li and the visiting scholar Donghui Li who help me a lot on my studying and living here.

At last, undoubtedly, many thanks to my family for always supporting me through all these years. Their love makes my life full of sunshine.

Summary

Dust or biomass burning particles coming from deserts such as Sahara in Africa have a great influence on the aerosols global emissions. The main purpose of this report is characterizing some of the night-time aerosol properties and variability in the Dakar site (Senegal). These properties including Aerosol Optical Depth (AOD), Ångström exponent (AE) α, Lidar ratio, Volume Size Distribution and vertical profile of extinction coefficient, are retrieved from ground-based measurements with lunar photometers and Lidar instruments.

First of all, I developed data processing software system to process the large databases. After that, more than four years of day and night continuous AOD and AE have been studied, which indicates the same annual cycle of variations with previous studies. Also the statistical results of Lidar ratio for dust cases over the year 2015 are presented, which shows good inversions at night-time. Then a reinforced verification of Lidar inversions at night-time is done by comparing CIMEL elastic Lidar inversions with Raman inelastic Lidar of several pure dust and dust-biomass mixed cases during Campaign SHADOW 2. Additionally, the recently developed algorithm and software GRASP-AOD is applied to retrieve size distribution at night-time, and the results show that GRASP-AOD can get a good retrieval of particle size in coarse mode.

1 Introduction

Aerosols are small particles suspending in the atmosphere which play an important role in human health and climate change. Knowing their composition and variability in time and space is of great value in understanding physical and chemical processes in the atmosphere. Desert dust is one of the major constituents of natural aerosol particles in the atmosphere. And as the largest dessert, the Africa Sahara is the primary dust source in global emission.[1] In 1996, the LOA (Laboratoire d'Optique Atmosphérique) in cooperation with the IRD (Institut de Recherche pour le Développement), started to conduct continuous observations in the Dakar (N14°23'38'', 16°57'32'') site.[2] In the past years, ground-based remote sensing system is this site was based on two main instruments, sun photometer and Lidar, to provide temporal and spatial variability of aerosols. However, aerosol may also change during night time. In recently years, lunar photometer was used to provide more information of aerosol optical properties and variability during night-time. In this work, we focused on the analysis of the night-time observations at this site over more than 4 years (from Jan, 2013 to Feb, 2017).

The main objectives of this work are as the following: 1, to study the annual variability of some aerosol properties retrieved from Sun-sky or Lunar photometers and Lidar instruments. 2, to verify the night-time measurements by comparing with daytime retrievals obtained from AERONET database and night-time observations using Raman Lidar during SHADOW 2 Campaign. 3, to retrieve volume size distribution of the night-time aerosols using the algorithm and software Grasp-AOD, using only the spectral AOD measured by lunar photometer.

The structure of the report is organized as follows: First of all, some conceptions and definitions used in this work are prepared in advance. Then instrumentation and methodology are introduced in section 3. In section 4, we present the data pre-processing method used for screening clouds data and software system developed to

process and display data automatically. And in section 5, results of aerosol properties including aerosol optical depth, Lidar ratio and volume size distribution are displayed and discussed. Finally, in section 6, we put forward some suggestions for further work.

2 Concepts and definitions

In this section, the concepts and definitions of some aerosol properties (such as optical depth, Ångström exponent, Lidar ratio and volume size distribution) used in this work will be introduced.

2.1 Aerosol optical depth and extinction coefficient

The direct sun irradiance measurements lead to the aerosol optical depth (AOD). AOD is an important parameter which describes the total column-integrated aerosol properties. The integrated relationship between AOD and the extinction coefficient $\sigma_{ext}(\lambda)$ is expressed as following:

$$\tau(\lambda) = \int_0^{z_{top}} \sigma_{ext}(\lambda, z)\,\mathrm{dz} \tag{2.1}$$

The extinction coefficient $\sigma_{ext}(\lambda)$ describes the extinction (scattering and absorption) ability of an ensemble of particles or molecules:

$$\sigma_{ext}(\lambda) = \sigma_{sca}(\lambda) + \sigma_{abs}(\lambda) \tag{2.2}$$

Where $\sigma_{sca}(\lambda)$ is the scattering coefficient of ensemble of particles. It is defined as the concentration of the particles per volume multiplied by the total cross section of one particle, namely

$$\sigma_{sca}(\lambda) = \int_0^{\infty} n(r)dr \times {\sigma_{sca}}^{1\_particle}(\lambda) \tag{2.3}$$

in which $n(r)$ is the particle size distribution.

The single scattering albedo (SSA) is the ratio of scattering coefficient to extinction coefficient:

$$\varpi_0 = \frac{\sigma_{sca}(\lambda)}{\sigma_{ext}(\lambda)} = 1 - \frac{\sigma_{abs}(\lambda)}{\sigma_{ext}(\lambda)} \tag{2.4}$$

when $\varpi_0 = 0$, it means all extinction due to absorption.

2.2 Ångström exponent

The relationship between size of atmospheric aerosols and wavelength dependence of extinction coefficient was first put forward by Ångström in 1929[3]. He obtained the useful Ångström empirical formula of Junge size distribution:

$$\tau(\lambda) = \beta \times \lambda^{-\alpha} \tag{2.5}$$

where β is the turbidity coefficient, and α is the Ångström exponent.

Ångström exponent α is an important parameter which reflects the aerosol size distribution. It is inversely related to the average size of the particles in the atmosphere: the smaller the particles, the larger the exponent. Based on the Ångström empirical formula, α can be retrieved by spectral AOD at two different wavelengths:

$$\alpha = -\frac{ln\frac{\tau_{\lambda_1}}{\tau_{\lambda_2}}}{ln\frac{\lambda_1}{\lambda_2}} \tag{2.6}$$

2.3 Volume Size Distribution

The lognormal Volume Size Distribution is often used to approximate particle size distribution of aerosols, defined as:

$$\mathrm{dv} = \mathrm{dV}/\mathrm{dlog(dr)} \tag{2.7}$$

For homogenous and spherical particles,

$$\mathrm{dv} = \frac{\mathrm{dV}}{\mathrm{dlog(r)}} = \frac{4}{3}\pi r^3 \frac{n(r)dr}{dlog(r)} = \frac{4}{3}\pi r^4 \mathrm{n(r)} \tag{2.8}$$

The relationship between the aerosol size distribution n(r) and the spectral AOD can be written as

$$\tau(\lambda) = \int_0^{\infty} \pi r^2 Q_{ext}(r, \lambda, m) n(r) dr \tag{2.9}$$

where $Q_{ext}(r, \lambda, m)$ is the extinction efficiency, defined as the extinction cross section normalized by the geometric cross section. And m is the complex refractive index of the aerosols.

In principle, under-certain assumptions (Torres et al., 2017)[4], the mathematical inversion of equation (2.9) can be done to retrieve the volume size distribution. Various methods have been proposed for solving this equation. King et al. built a model which

only uses spectral AOD to invert aerosol properties[5]. The method of Nakajima et al. is used to retrieve aerosol properties using sky-scan radiance with or without spectral AOD[6][7]. Then Dubovik et al. put forward an inversion method using both spectral AOD and sky-scan radiance[8], and this method has been used in the Aerosol Robotic Network (AERONET).

2.4 Extinction-to-backscatter ratio

Extinction to backscatter ratio, also called Lidar ratio, is defined as

$$S_a = \frac{\sigma_{a,ext}}{\beta_a} \tag{2.10}$$

where β_a is the aerosol backscatter coefficient given by

$$\beta = \sigma_{sca}.p(180°)/4\pi \tag{2.11}$$

Then equation (2.10) and (2.11) yield,

$$S_a = \frac{4\pi\sigma_{a,ext}}{\sigma_{sca}.p(180°)} = \frac{4\pi}{\varpi_0 p(180°)} \tag{2.12}$$

Lidar ratio typically varies from as low as 10 to about 100 sr, depending on the type of particles[9][10] as shows in equation (2.12). Figure 2-1 shows the Aerosol type model classified by Lidar ratio and the particle depolarization ratio at 532nm.

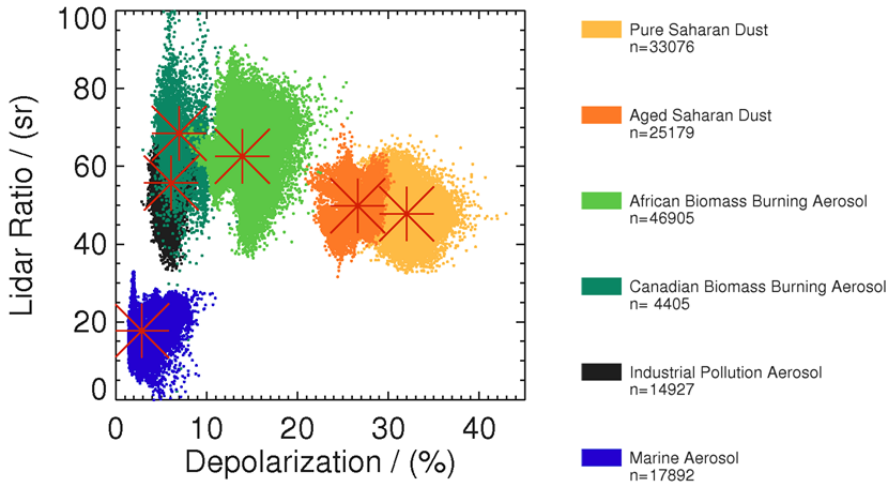

Figure 2- 1 Aerosol classification classified by Lidar ratio and depolarization ratio at 532nm (Petzold et al., 2009) [11] according to LiDAR Raman night-time observations.

The depolarization ratio in this figure is linked to several elements of scattering matrix and is closely related to shape of particles. It can measured by certain Lidar

technology. Using this model, we can infer aerosol types in one specific region after retrieve Lidar ratio from ground measurements.

3 Instrumentation and Methodology

Both passive and active remote sensing instruments are used at Dakar site to perform ground based observations. In this part, we introduce briefly these instruments and the related methodology used to retrieve some optical properties.

3.1 Sun-sky photometer and moon photometer

The standard CE-318 Sun photometers can measure the direct solar radiation transmitted through the integral atmosphere column and the sky-scan radiance at several scattering angles automatically. These measurements are collected at several wavelengths, from UV to the near-infrared spectral domain, which are centered in 340, 380, 440, 500, 675, 870, 1020, 1640nm. Based on this instrument, the Aerosol Robotic Network (AERONET) was first built in 1996 to get the global observation of aerosols during daytime.

For the night-time aerosol monitoring, we use lunar photometry to perform direct atmospheric transmission. The pioneering work in moon photometry is conducted by Berkoff et al. who use a modified Cimel Sun photometry to obtain the spectral AOD with the moon as light source[12]. In 2013, Barreto et al. presented a new photometer prototype (CE318-U) to perform lunar measurements to characterize aerosols and water vapour at night-time[13]. CE318-U was able to perform nocturnal measurements under a moon illumination greater than 50%. Then in 2016, they improved their technique by designing a new sun-sky-lunar photometer CE318-T, which can perform both daytime and night-time photometric measurements using the sun and moon as light source[14]. Thus, a complete cycle of diurnal aerosol and water vapour monitoring can be performed with only one instrument.

In the Dakar site, lunar photometry CE318-U (2013-1015) and CE318-T (2016) are used to perform night-time aerosol monitoring. The current effective wavelengths are centered at 440, 500, 670, 870, 1020 and 1640 nm. Figure 3-1 shows the day and night continuous measurements of AOD and AE.

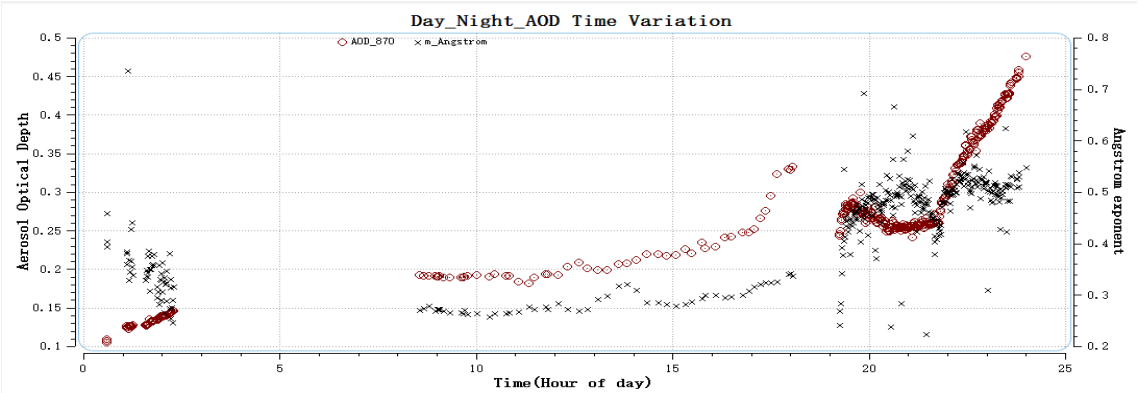

Figure 3-1 AOD and AE daily variations

We can see that in this case aerosols changed a lot at night-time. Hence, to keep more information of aerosols, it's necessary to perform night-time aerosol observations with lunar photometer.

3.2 Elastic-backscatter Lidar and Raman Lidar

3.2.1 Instruments introduction

Passive optical remote sensing methods using radiation from sun or moon don't provide the information of how aerosol properties are distributed with altitude. In this case, Light Detection and Ranging (Lidar) technique was introduced to profile the atmosphere. As an active instrument in situ, Lidar provides measurements of tropospheric vertical optical properties of aerosol and clouds layer with high spatial (3m) and temporal (3 minutes) resolution. High spatial and temporal resolution, the possibility of observing atmosphere at ambient conditions, and the potential of covering the height range from the ground to more than 100km altitude (some few of them) make up the attractiveness of Lidar instruments.[15]

In this work, we use Dakar Elastic Backscatter Lidar database to screen clouds

data in lunar AOD database, and to analyze the extinction-to-backscatter ratio (Lidar ratio), and compare with the ones obtained from independent Raman Lidar measurements when possible. The cloud screening is an important issue that is much more complicated for night-time than daytime where additional sky radiance helps to separate aerosol and clouds, especially cirrus clouds. This is the reason why we improved the cloud screening in considering with the Lidar cloud detection.

Raman scattering is an inelastic scattering process which involves the change of the vibrational-rotational energy level of molecule. The change of the vibrational energy level results in frequency shifts of a few hundred to several thousand wavenumbers depending on the Raman-active molecule. Spectrally resolved analysis of backscattered radiation allows in principle the detection of a variety of atmospheric species[15]. Here we only focus on the application of Raman Lidar in extinction profiles and Lidar ratio retrieval. Sun photometer measurements describe the entire integrated vertical column, which can bias aerosol properties retrieved by combining elastic backscatter Lidar and Sun photometer in situations with inhomogeneous aerosols. In this work, we use Raman Lidar results obtained during SHADOW 2 Campaign to compare the extinction profiles and Lidar ratio with elastic-backscatter Lidar.

The main backwards of Raman Lidar is low SNR (Signal and noise ratio) of daytime measurements, so at present Raman Lidar can only meet quality requirements at night-time. And lunar photometer enables us to compare elastic-backscatter Lidar retrieval with Raman Lidar. The results will be presented in Part 5.

3.2.2 Lidar equations

As we referred before, Lidar can provide the vertical distribution information of particles in the atmosphere. The backward scattering light is detected and amplified, extinction coefficient profile can be obtained using BASIC algorithm (Mortier et al., 2013) from backscattered laser power[16]. In this unit, we will introduce the typical solutions of elastic-backscatter Lidar and Raman Lidar equations separately.

3.2.2.1 Elastic Lidar equation

In the elastic channel, the received signal $X(\lambda)$, which is the received power $P_d(\lambda)$ corrected by the detecting range, can be expressed as

$$X(z) = P_d(z)z^2 = A(\lambda)(\beta_a(z) + \beta_{mol}(z))\exp(-2\int_{z_{min}}^{z}(\sigma_{a,ext}(z') + \sigma_{mol}(z'))dz') \quad (3.1)$$

where $A(\lambda)$ is the measured data and an instrumental constant.

There are several methods published to invert elastic Lidar signal. The most widely used one is Klett method from which the BASIC algorithm is inspired. This method uses extinction to backscatter ratio to reformulate the Lidar equation. As a result, Lidar equation can be formulated using S_a and β_a

$$X(\lambda) = A(\lambda)(\beta_a(z) + \beta_{mol}(z))\exp(-2\int_{z_{min}}^{z}(S_a\beta_a(z') + \sigma_{mol}(z'))dz') \quad (3.2)$$

In this equation, for a chosen reference height z_{ref}, $\beta_m(\lambda, z_{ref}) \gg \beta_a$, so $\beta_a(z)$ can be considered as 0. $\beta_{mol}(z)$ and $\sigma_{mol}(z)$ can be pre-calculated according to the reference molecule and wavelength of Rayleigh scattering. As a conclusion, we have one equation but two unknown variables $S_a(z)$ and $\beta_a(z)$. In Klett method, $S_a(z)$ is set a constant (meaning the aerosols layer is supposed to be homogeneous in type), thus we can retrieve $\beta_a(z)$. According to the definition of Lidar ratio, aerosol extinction vertical profile can be retrieved.

3.2.2.2 Raman inelastic Lidar equation

Raman Lidar equation can be expressed as：

$$X(\lambda_R, z) = A(\lambda_R)(\beta_m(\lambda_R, z) + \beta_a(\lambda_R, z))\exp\left(-\int_{z_{min}}^{z}\left(\sigma_a(\lambda, z') + \sigma_m(\lambda, z') + \sigma_a(\lambda_R, z') + \sigma_m(\lambda_R, z')\right)dz'\right) \quad (3.3)$$

where λ_R is the wavelength of Raman scattering. R represents the reference molecule, for example N_2, O_2, water vapor and so on. For a chosen reference height z_{ref}, $\beta_m(\lambda, z_{ref}) \gg \beta_a(\lambda, z_{ref})$, so $\beta_a(\lambda, z_{ref})$ can be considered as 0.

In this equation, $A(\lambda_R)$ is considered as constant, Raman backscattering coefficient $\beta_R(\lambda_R, z)$ and molecule elastic and inelastic extinction coefficients $\alpha_m(\lambda, z') + \alpha_m(\lambda_R, z')$ are pre-calculate according to the reference molecule and wavelength of Raman scattering. So only aerosol elastic and inelastic extinction coefficients $\sigma_a(\lambda, z') + \sigma_a(\lambda_R, z')$ need to be determined. According to the definition of Ångström exponent we have referred before, $\sigma_a(\lambda, z')$ and $\sigma_a(\lambda_R, z')$ can be linked by Ångström exponent α, which is defined as

$$\frac{\sigma_a(\lambda,z')}{\sigma_a(\lambda_R,z')} = \left(\frac{\lambda}{\lambda_R}\right)^{-\alpha} \tag{3.4}$$

Thus, the Raman Lidar equation is solved.

Klett method used to solve elastic-backscatter Lidar assumes that Lidar ratio S_a is a constant, however, in fact S_a is not always a constant but depends on the aerosol type and distribution. At this point, Raman Lidar has the advantage, however, as we said before, it can only meet acquirements at night-time

4 Data pre-processing and software system

4.1 Data pre-processing

The spectral AOD measured by lunar photometer should be firstly filtered by moon Fraction Index (FI) larger than 0.5 to ensure the accuracy can meet requirements. FI is the luminous degree of the moon, ranges from 0 to 100%. Hereafter, we need to use AOD triplet variability to detect clouds. A triplet corresponds to three successive AOD measurements within 1 min. In this work, we screen clouds by set thresholds for absolute ($\Delta AOD<0.01$) and relative value ($\Delta AOD/AOD<0.008$) of triplets. Figure 4-1 shows one case which successfully screens clouds data using this method.

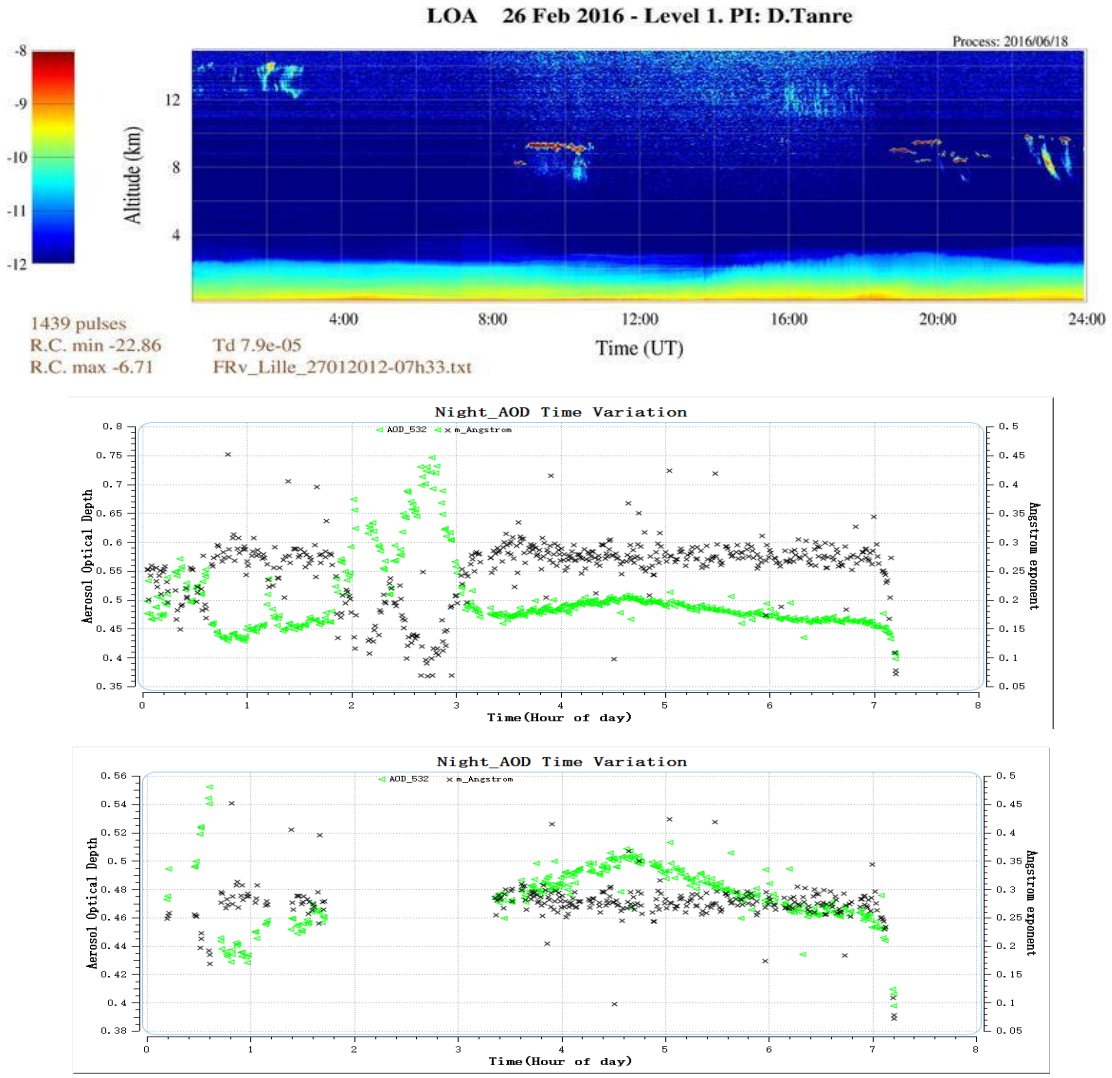

Figure 4- 1 Clouds screened succeeded case on Feb 26th, 2016. The three figures are: Lidar "Quick Look", AOD at 532 nm (green) and AE (black) before cloud screening, AOD and AE after cloud screening.

We can see that AOD between 2h to 3h20 are removed, and the Lidar Quick Look in figure 4-2 shows that there are high altitude clouds in this period. This method can detect out most of the thick clouds, but it doesn't always work well. For example, when there are thinner clouds and last for a long time, this method is limited, see figure 4-2.

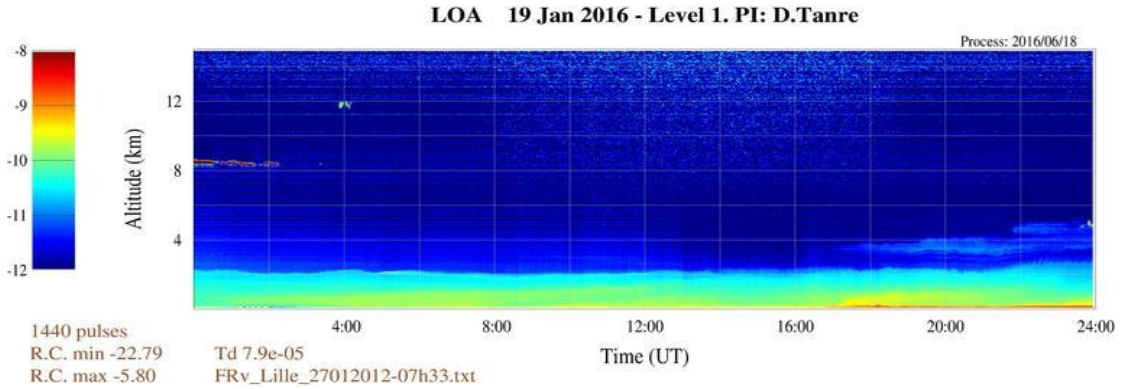

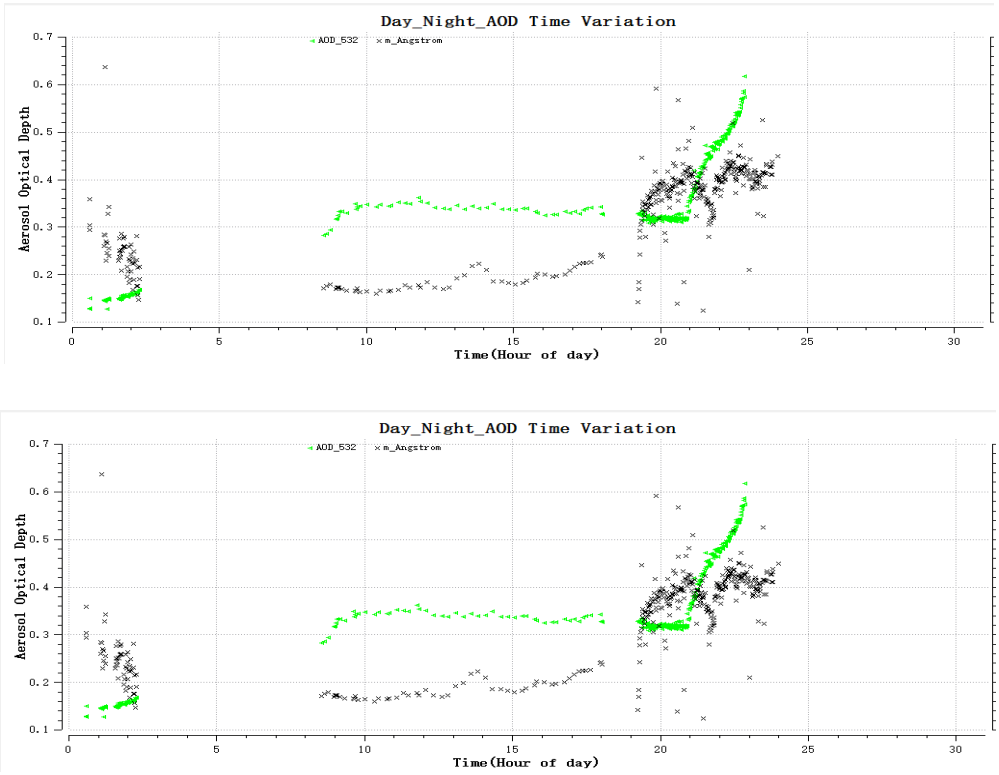

Figure 4-2 Clouds screened failed case on Jan 19th, 2016

4.2 Software system

The ground based remote sensing measurement data from year 2013 to year 2017 used in this work is huge. Day-time AOD and Lidar measurements data used in this work can be easily accessed from AERONET website and Lidar-LOA website. The night-time AOD also have been retrieved from Moon photometer. To analysis and display these huge databases automatically, I developed data processing software system during my internship.

Firstly, two SQLite databases have been established. Day and night AOD data retrieved from Sun-sky photometer and Moon photometer are all integrated into one database '2013_2017_AOD'. Lidar ratio as well as AOD at 532nm wavelength used in the Lidar retrieval are also insert into the other database '2013_2017_Lidar'. Various data tables are created in the two databases to store and classify data for different usage. Secondly, since statistics analysis in different time spans is frequently needed in this work, the software system can also calculate and display data in real time. Time span

choosing box is provided on the software interface. The two interfaces of AOD data processing software and Lidar data processing software are listed below.

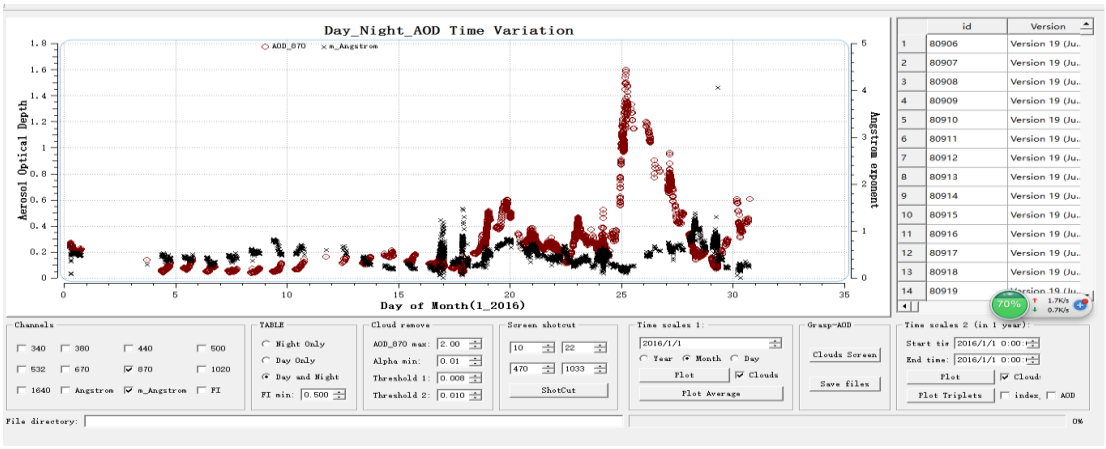

Figure 4- 2 Interface of Lunar photometer database processing software

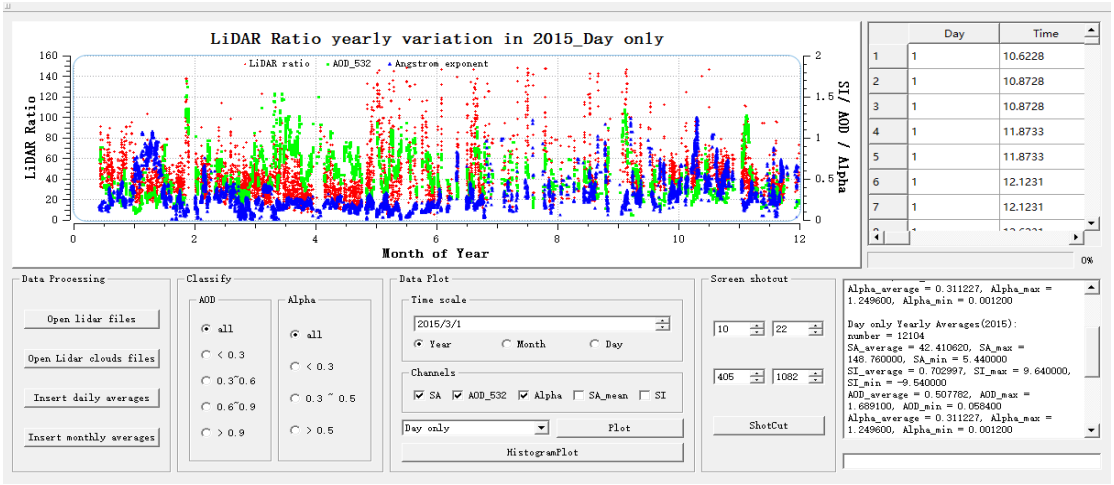

Figure 4- 3 Interface of Cimel-Lidar database processing software

In the next section, we will present our results and make some comments.

5 Results and Discussion

More than four years of continuous aerosol observations performed at Dakar have been analyzed in this work. In this part, we will present some aerosol properties retrieved from these complementary observations and provide analysis of the results. Firstly, the statistical analysis of column integrated properties such as aerosol optical depth and Ångström exponent are presented in different time scales, which can indicate the

temporal variability of aerosols at Dakar site. Secondly, we analysis more specifically the extinction-to-backscatter ratio (Lidar ratios) which is related to aerosol types. The volume size distributions of some dust cases are retrieved using the recently developed software Grasp-AOD.

5.1 Aerosol optical depth (AOD) and Ångström exponent (AE)

Studying the temporal variability of AOD and AE is of great value in knowing the climatology of aerosol properties and temporal tendency at this site. AOD and AE time variations in different time scales (typically one month or one year) are presented in this section.

AOD at 532nm and AE retrieved from daytime and night-time measurements in one month (January, 2016) are gathered in figure 5-1.

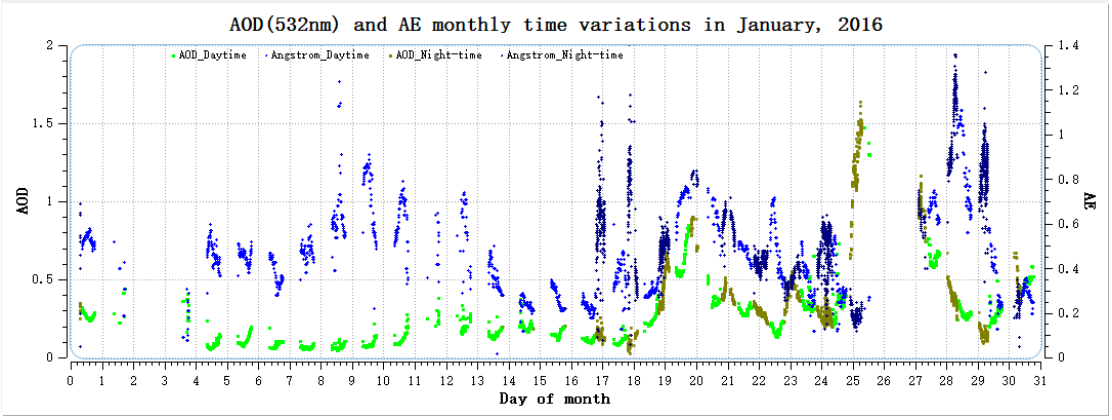

Figure 5- 1 AOD (532nm) and AE daytime variations in January, 2016. The light green and light blue one are AOD(see values from y-left axis) and AE(see values from y-right axis) in daytime. The dark green and dark blue are those in night-time.

From figure 5-1 we can see that, aerosols vary a lot in this month, both AOD and AE. AOD increased fast since Jan 25th and reached a peak value on Jan 26th, then fell down to a point lower on Jan 30th. While at the same time, the Ångström exponent changed reversely with AOD. More precisely, on Jan 26th, at Dakar site, AOD was very high while AE was low (less than 0.3), which indicated desert dust was dominating. On the opposite, a couple of days later, AOD are lower but AE increase, this could very likely be due to biomass burning particles transported over Dakar.

Focus on the night-time measurements effective days from 17th to the end of this month (figure 5-2), we can find that the night-time AOD and AE variations has the same trend of change with daytime AOD variations. This can prove the validity of our night-time measurements to some extent. As a result, we obtained effective and constructive AOD measurements during day and night in this month. Table 2 show the averages of AOD and AE in this period. We can notice that, AE average value is around 0.5, so very probably that biomass burning particles are dominating in this period. And AOD and AE standard deviation are high, which indicates big variability of aerosols.

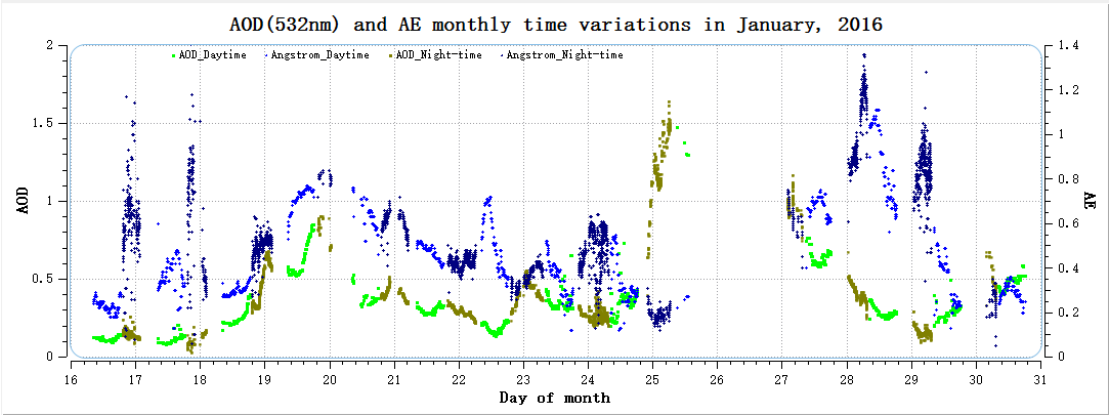

Figure 5- 2 AOD and AE time variations

Table 5- 1 Table of averages and standard deviations (Jan 17th ~ Jan 31th , 2016)

Day or night	Number	AOD		AE	
		Average	Standard deviation	Average	Standard deviation
Daytime	1477	0.33	0.178	0.46	0.212
Night-time	6607	0.37	0.247	0.55	0.234
Day-night	8084	0.36	0.238	0.53	0.233

In order to investigate the long-term variability of aerosol variability at Dakar site, monthly averages and daily averages of AOD at 870 (because of missing data in 532nm) on the whole observation time scale, from Jan, 2013 to Feb, 2017 are computed, see figure 5-3. Averages and standard deviations of AOD (532nm) and AE over the whole time scales are list in table 5-2.

The AOD annual cycle can be found in figure 5-3. AOD always reaches its maximum value in summer and minimum value in winter. While on the contrary, Ångström exponent has its maximum value in winter and minimum value in summer. So we can infer that, at Dakar site, there are lots of coarse particles such as desert dust

in summer, while in winter finer particles such as biomass burning are dominating. The large values of standard deviations both AOD and AE in table 5-2, also show very big variability of aerosols in Dakar site. An overall average of AE of 0.366±0.253 infers that the coarse mode is dominating. These results agree well with the conclusions put forward by Mortier, et al.[2], who studied nearly a decade of daytime aerosol observations performed at Dakar site, from year 2003 to 2014.

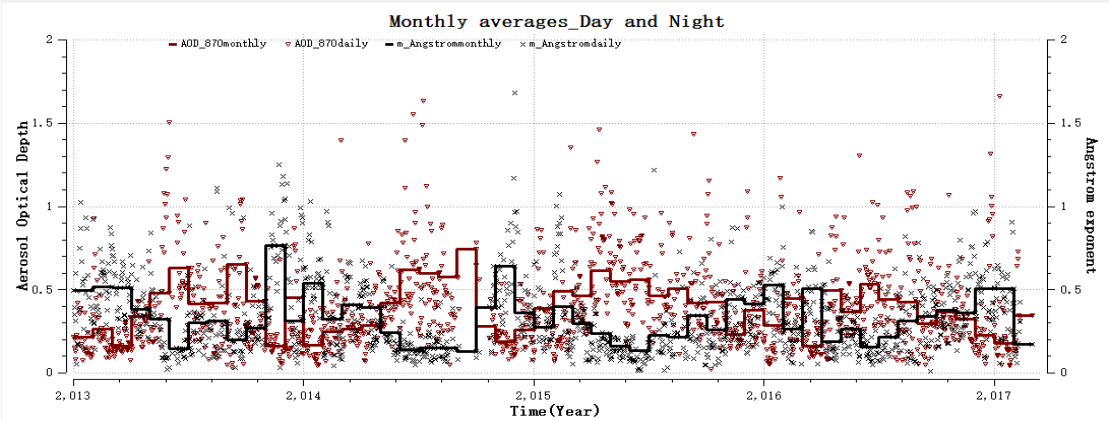

Figure 5- 3 Monthly averages (steps) and daily averages (dots) of AOD and AE from Jan, 2013 to Feb, 2017.

Table 5- 2 Table of averages and standard deviations (Jan, 2013 ~ Feb, 2017)

Day or night	Number	AOD (532nm)		AE	
		Average	Standard deviation	Average	Standard deviation
Daytime	74934	0.4	0.236	0.37	0.262
Night-time	81936	0.39	0.239	0.36	0.244
Day-night	156870	0.39	0.238	0.37	0.253

5.2 Extinction to backscatter ratio

As we have referred in section 2.4, Lidar ratio has close relationship with aerosol types, and in Dakar site, the atmosphere is been influenced by desert dust all the year-round. Therefore, in this section we will focus on the study of desert dust cases in Dakar site by studying the corresponding Lidar ratios retrieved from Cimel elastic Lidar.

Here we present the annual Lidar ratio time variation in 2015 in figure 5-4. These Lidar ratios are firstly filtered by Slope index between 0.9 and 1.1. The slope index here is an indication on how well the Lidar signal fits the molecular profile in chosen molecular zone, 1 means good quality inversion. Then since we focus on dust situations,

a second constrain is put on Lidar ratio (AE below 0.3), Detailed information about Lidar ratio distributions separated by day and night as well as their average values see figure 5-5 and table 5-3.

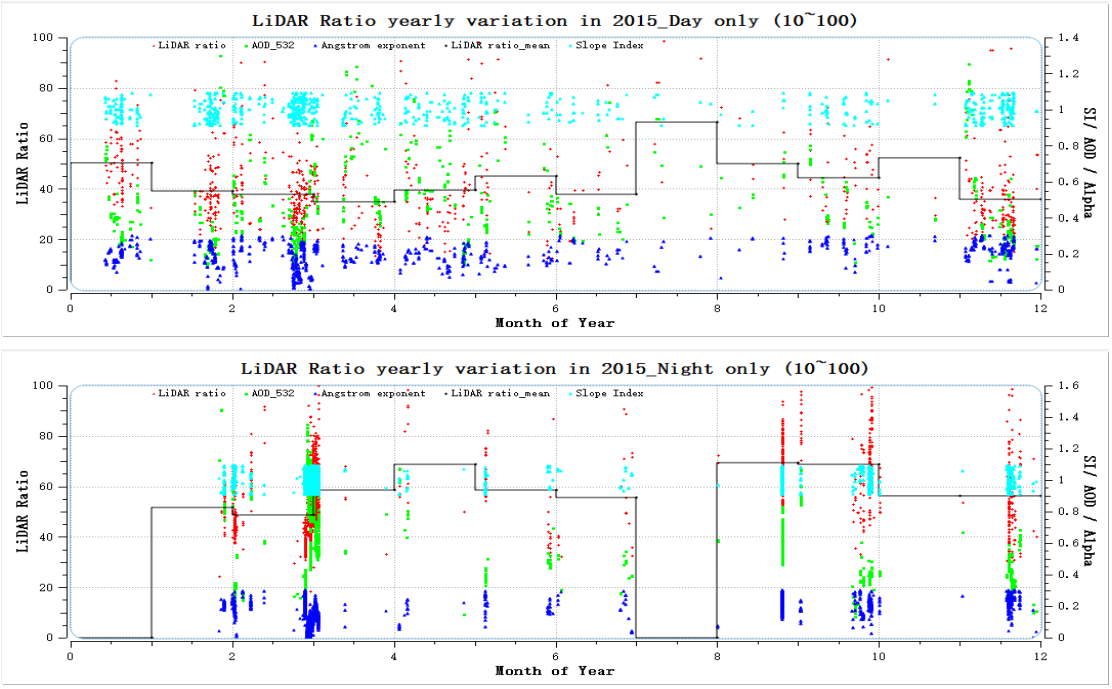

Figure 5- 4 Daytime and night-time yearly variations (red dots) and monthly averages (black steps) of Lidar ratio time in 2015 at Dakar site. Except for Lidar ratio, AOD at 532nm (green dots) and Ångström exponents (blue dots) are also presented in this figure.

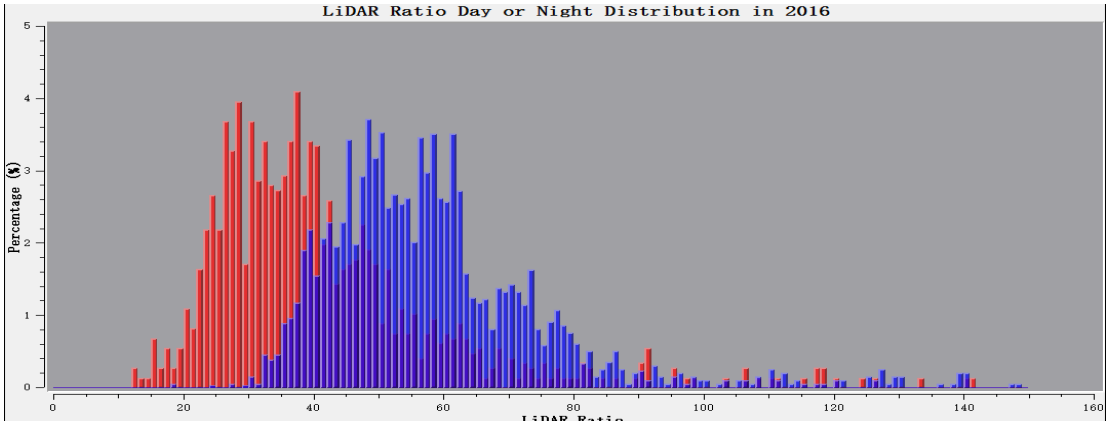

Figure 5- 5 Day (red) and night (blue) Lidar ratio distribution in 2015 (Ångström < 0.3).

Table 5- 3 Statistical results of Lidar measurements in 2015 at Dakar site

Day or night	Number	Mean value		
		SA	AOD	Alpha
Day and night	22846	49.4	0.47	0.33
Day only	7894	40.9	0.42	0.34
Night only	14952	53.9	0.2	0.33

According to aerosol type model in figure 2-1, Lidar ratio of pure dust range

between 36~64 sr and centered at 49-50 sr. From figure 5-5 we can see that, most of the monthly averages of Lidar ratio both in daytime and night-time fit the value of dust. While from the Lidar ratio distribution histograms one can note that Lidar ratios retrieved from daytime measurements are systematically lower than expectation. An explanation for the lower Lidar ratio values by day could be that the automatic detection of the reference altitude (molecular) by day is difficult for the algorithm when AOD is high, and at 5-6 km of the altitude the Lidar signal is already noisy.

In order to analyze more deeply, we also compared the extinction coefficient profiles and Lidar ratio retrieved from elastic Lidar with those retrieved from Raman inelastic Lidar. Several pure dust cases and dust-biomass mixed cases with relatively higher AOD are studied in this work. The results are show in table 5-2 and table 5-3. Since accumulation time is also important for CIMEL Lidar inversion, here we take two different accumulation time (10 and 60 minutes) as references.

Table 5- 4 Lidar ratios retrieved from elastic and inelastic Lidar for pure dust cases

Date/Time (Raman)	**CIMEL**		**Raman**	**AOD**	**Ångström**	**FI**
2015	10min	60min				
0330-00H	56.1	57.5	54.4	0.83	0.08	0.75
0331-00H-01H30	49.1	68.4	50.3	1.08	0.0038	0.83
0329-22H-23H30	57.5	55.6	53.0	1.19	0.0358	0.75
0330-22H30-24H00	50.4	43.4	54.4	0.74	0.0578	0.83
0401-20H-21H30	57.4	62.9	57.9	0.7	0.187	0.94
0401-23H30-24H00	63.8	58.0	55.1	0.62	0.198	0.94
0402-00H-01H30	57.8	60.9	59.1	0.56	0.181	0.95
0402-02H-04H	59.7	56.4	54.9	0.54	0.189	0.95

Table 5- 5 Lidar ratios retrieved from elastic and inelastic Lidar for dust-biomass cases

Date/Time (Raman)	**CIMEL**		**Raman**	**AOD**	**Ångström**	**FI**
2016	10min	60min				
0117 20H-22H	56.1	57.5	54.4	0.83	0.08	0.75
0119 20H-22H	49.1	68.4	50.3	1.08	0.0038	0.83
0119 22H-24H	57.5	55.6	53.0	1.19	0.0358	0.75
0120 02H-04H	50.4	43.4	54.4	0.74	0.0578	0.83
0122 23H-01H	57.	62.9	57.9	0.7	0.187	0.94

From the tables we can see that, most of the Lidar ratios obtained by elastic Lidar inversion agree well with Raman inelastic Lidar inversions. To know more details about

those bad inversions, here we present the extinction profiles and Lidar ratios obtained from CIMEL elastic Lidar and Raman inelastic Lidar for four good inversions and two bad inversions, see figure 5-7 and figure 5-8. Comparing these cases one can notice that, CIMEL Lidar can have a better inversion when there is a homogenous and thin layer of aerosols, figure 5-7. However when the aerosols extinction coefficient varies a lot with the height, the inversions are not so good. This can be explained by the different methods for solve Lidar equations (see 3.2 section). For CIMEL Lidar, the Lidar ratio is vertically constant, while Raman Lidar can provide the vertical profile of Lidar ratio.

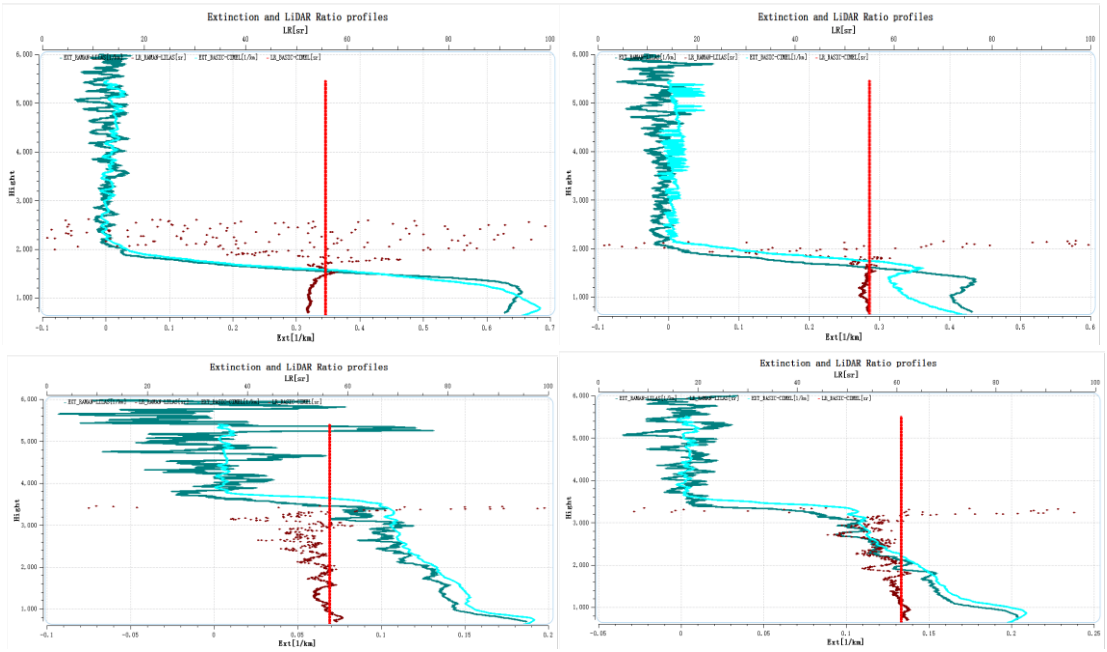

Figure 5- 6 Extinction profiles and Lidar ratios of good inversion cases.

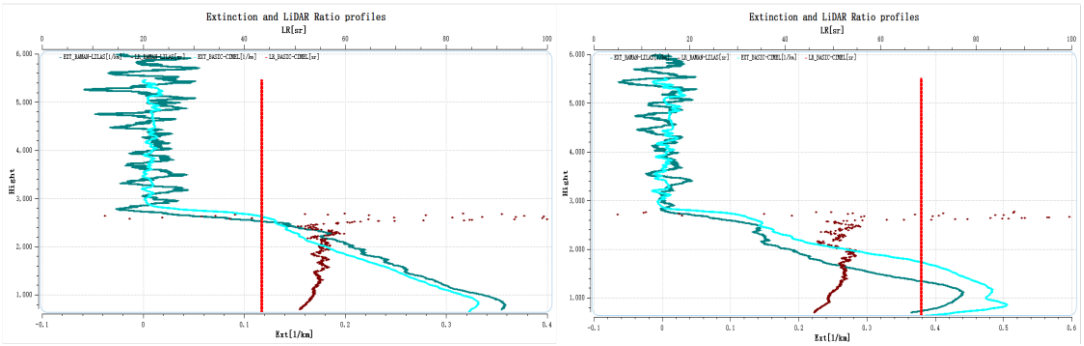

Figure 5- 7 Extinction profiles and Lidar ratios of bad inversion cases.

5.3 Volume Size distribution

As we have already known, VSD can be inferred from spectral AOD complemented

with sky scattering information at different wavelengths. The spectral AOD can be obtained by direct measurements of Sun/Lunar photometer, but unfortunately, sky-scan radiance is unavailable for lunar photometry since the illumination of moon light is too weak to provide measurable sky radiance. However, since AOD over different wavelengths is related to the amount and size distribution of aerosols, it's potential to retrieve volume size distribution for night-time measurements using spectral optical depth measurements.

In this work, we used GRASP-AOD developed by Torres et al[4] to retrieve nocturnal VSD (and daytime). To evaluate of the algorithm of GRASP-AOD, we also applied this algorithm to the spectral AOD measured by Sun photometer. Thus we can compare the VSD obtained by GRASP-AOD with those retrieved by Dubovik et al[8].

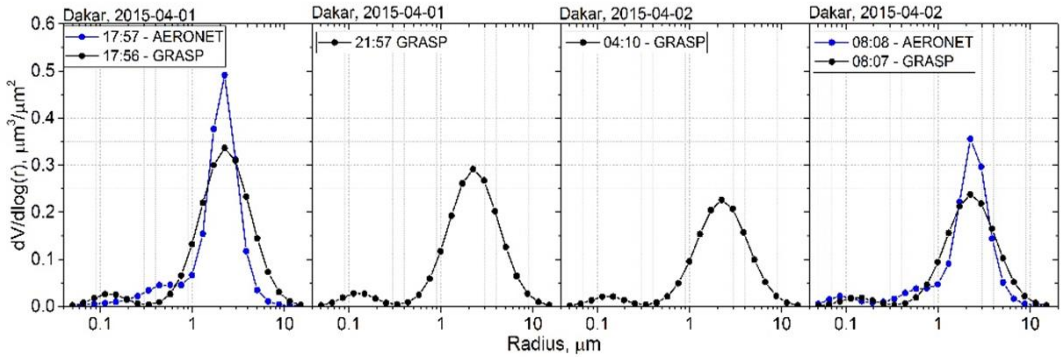

Figure 5- 8 Size distributions retrieved from GRASP-AOD (dark) and AERONET (blue).

We compare the daytime size distributions retrieved by GRASP-AOD and AERONET, we can note that, for coarse mode, particle size are well retrieved, while for the fine mode, the radius is not centered on the same value. However, the amplitude of the fine mode is very small (small amount of fine particles). The amplitude for the coarse mode is under-estimated by GRASP-AOD as announced by Torres et al., since the sensitivity of AOD to coarse mode particles is less than that for fine particles.

6 Conclusions and perspectives

A first analysis of some aerosol properties at Dakar site in recently 4 years has been

done in this work. An overall average of AOD (532nm) of 0.4 ± 0.2 and AE of 0.37 ± 0.26 indicate that there is a high aerosol loading with a big variability in the Dakar site. And coarse mode (low AE) are dominating all the year round. The annual aerosol variations also show that biomass burning increase a lot in the wintertime. Besides, nocturnal measurements with Lunar photometer have been proved to be able to provide available information on aerosol properties, either by comparing with AERONET database or Raman Lidar retrievals. To process data automatically, I developed software system which greatly improved our work efficiency.

Several questions have also been raised during our work. Firstly, to provide more information of aerosols properties in this site, other optical properties need to be analyzed in the further work.

Secondly, the quality of daytime Lidar inversions need to be improved because of the lower Lidar ratio distributions. And when aerosols have a big vertical variability, elastic-backscatter Lidar is less reliable on Lidar ratio inversions.

Additionally, in this work, Volume Size Distribution is only analyzed in several pure dust cases, and this is done case by case. Since continuous measurements are performed almost every night, automatically processing system should be built to retrieve the nocturnal VSD.

Furthermore, at present, fine mode VSD in our cases (dust) can’t be retrieved correctly from only spectral AOD, so observation system at night-time need to be improved to provide more information of aerosol properties.

References

[1]Wagner F, Bortoli D, Pereira S, et al. Properties of dust aerosol particles transported to Portugal from the Sahara desert[J]. Tellus B, 2009, 61(1): 297-306.

[2] Mortier A, Goloub P, Derimian Y, et al. Climatology of aerosol properties and clear‐sky shortwave radiative effects using Lidar and Sun photometer observations in the Dakar site[J]. Journal of Geophysical Research: Atmospheres, 2016, 121(11): 6489-6510.

[3] Ångström A. On the atmospheric transmission of sun radiation and on dust in the air[J]. Geografiska Annaler, 1929, 11: 156-166.

[4] Torres B, Dubovik O, Fuertes D, et al. Advanced characterization of aerosol properties from measurements of spectral optical depth using the GRASP algorithm[J]. Atmos. Meas. Tech. Discuss, 2016.

[5] King M D, Byrne D M, Herman B M, et al. Aerosol size distributions obtained by inversions of spectral optical depth measurements[J]. Journal of the atmospheric sciences, 1978, 35(11): 2153-2167.

[6] Nakajima T, Tanaka M, Yamauchi T. Retrieval of the optical properties of aerosols from aureole and extinction data[J]. Applied Optics, 1983, 22(19): 2951-2959.

[7] Nakajima T, Tanaka M. Algorithms for radiative intensity calculations in moderately thick atmospheres using a truncation approximation[J]. Journal of Quantitative Spectroscopy and Radiative Transfer, 1988, 40(1): 51-69.

[8] Dubovik, O., & King, M. D.. A flexible inversion algorithm for retrieval of aerosol optical properties from Sun and sky radiance measurements. *Journal of Geophysical Research: Atmospheres*, 2000, *105*(D16), 20673-20696.

[9] Cattrall C, Reagan J, Thome K, et al. Variability of aerosol and spectral Lidar and backscatter and extinction ratios of key aerosol types derived from selected Aerosol Robotic Network locations[J]. Journal of Geophysical Research: Atmospheres, 2005, 110(D10).

[10] Groß S, Esselborn M, Weinzierl B, et al. Aerosol classification by airborne high spectral resolution Lidar observations[J]. Atmospheric chemistry and physics, 2013, 13(5): 2487-2505.

[11] Petzold A, Rasp K, Weinzierl B, et al. Saharan dust absorption and refractive index from aircraft-based observations during SAMUM 2006[J]. Tellus B, 2009, 61(1): 118-130.

[12] Berkoff T A, Sorokin M, Stone T, et al. Nocturnal aerosol optical depth measurements with a small-aperture automated photometer using the moon as a light source[J]. Journal of Atmospheric and Oceanic Technology, 2011, 28(10): 1297-1306.

[13] Barreto A, Cuevas E, Damiri B, et al. A new method for nocturnal aerosol measurements with a lunar photometer prototype[J]. Atmospheric Measurement Techniques, 2013, 6(3): 585-598.

[14] Barreto A, Cuevas E, Granados-Muñoz M J, et al. The new sun-sky-lunar Cimel CE318-T multiband photometer–a comprehensive performance evaluation[J]. Atmospheric Measurement Techniques Discussions, 2015, 8: 11077-11138.

[15] Wandinger U. Introduction to lidar[M]//Lidar. Springer New York, 2005: 1-18.

[16] Mortier A, Goloub P, Podvin T, et al. Trends and variability of aerosol vertical distribution and properties using micro-LIDAR and sun-photometer measurements[C]//Cahalan R F, Fischer J. AIP Conference Proceedings. AIP, 2013, 1531(1): 508-511.